Three-Dimensional Gravity Inverse Modeling for Basement Depth Estimation Integrating Maximum Difference Reduction (MDR), Trend Surface Analysis (TSA) and Total Variation Regularization

Accep Handyarso[1,2,*] & Hendra Grandis[2,3]

[1]Geophysics Group, Centre of Geological Survey, Indonesia Geological Agency, Building B 1st Floor, Jalan Diponegoro 57, Bandung 40122, Indonesia.
[2]Graduate Program in Geophysical Engineering, Basic Science Center B 2nd Floor, Jalan Ganesha 10, Bandung 40132, Indonesia.
[3]Faculty of Mining and Petroleum Engineering, Institut Teknologi Bandung, Basic Science Center B 2nd Floor, Jalan Ganesha 10, Bandung 40132, Indonesia.
*E-mail: accep.handyarso@esdm.go.id

Abstract. In sedimentary basin studies, gravity data are typically used to estimate the basement topography. Gravity inversion methods are expected to be able to discriminate between continuous and discontinuous sedimentary basins. Most 3D gravity inversion methods require intensive computational resources (computer memory and processing time). MDR3D, a variant of the well-known Bott method, was transformed into the Gauss-Newton inversion approach for extension flexibility. Integration of trend surface analysis (TSA) into the inversion scheme for regional anomaly estimation allows basement depth estimation from the Bouguer anomaly data. The aim of the additional total variation regularization is to stabilize the inversion algorithm and to achieve a geologically feasible model, especially for discontinuous basin types. Evaluation of the proposed method led to satisfactory results both for the synthetic and the field data set. It was found that the regularization parameter can improve the stability of the algorithm and also the depth estimation from noisy data up to ±0.5 mGal.

Keywords: *basement depth; Bouguer anomaly; Gauss-Newton; MDR3D; regional-residual anomaly; trend surface analysis (TSA); total variation regularization.*

1 Introduction

In preliminary studies of sedimentary basins, the gravity method is commonly used to infer the sediment thickness or the basement depth. The gravity data interpretation involves an inverse modeling algorithm. Bott [1,2] was among the first to introduce a kind of inversion algorithm to estimate two-dimensional (2D) sediment thickness from gravity data. The first estimate of the sediment thickness and its iterative modifications are both based on the Bouguer slab approximation. In this case, the 2D gravity forward modeling for an *N*-sided

Received December 12th, 2016, 1st Revision April 25th, 2017, 2nd Revision June 19th, 2017, Accepted for publication August 15th, 2017.
 ISSN: 2337-5779, DOI: 10.5614/j.eng.technol.sci.2017.49.3.5

polygon is used to evaluate the model response fitness with respect to the observed data [2]. Other approaches of gravity forward modeling and inverse modeling in the spatial frequency domain have been proposed by Parker [3] and Oldenburg [4]. However, the resulting solutions were not stable, so that the concept of Tikhonov regularization was introduced to stabilize the computation process [5,6]. In its applications, the Tikhonov regularization has several variants, such as smoothness, total variation, minimum support, gradient minimum support, minimum entropy, etc. [6,7].

It is possible to formulate the algorithm proposed by Bott in the form of the Gausss-Newton inversion method, where the Jacobian matrix is based on the Bouguer slab formula. Thus the concept of regularization and also constraints can be added into the Bott method [6]. The regularization method most commonly used is smoothing. Smoothing regularization improves the depth estimation result and at the same time stabilizes the inversion process. This regularization is suitable only for geological conditions that are relatively smooth, such as in intracratonic basins. However, there are basins with steep faults, for example in rifting basins, where smoothing regularization is considered not appropriate. In such cases, total variation regularization is considered more feasible from a geological point of view. Total variation regularization basically maintains the minimum sum of the lateral changes of the subsurface model according to the total variation stabilizing function in the form of L_1-norm [8,9].

The maximum difference reduction (MDR) method has been applied successfully for 2D sedimentary basins [10]. The MDR method for 3D sedimentary basins was developed by employing the 3D gravity forward modeling from Blakely [2]. We reformulated the MDR3D algorithm in the form of the Gauss-Newton inversion method to allow the implementation of trend surface analysis (TSA) to solve the subjectivity problem during regional-residual anomaly separation [11,12]. In addition, we also incorporated constraints as well as the total variation regularization concept in the same inversion scheme.

2 The Algorithm

2.1 Forward Modeling

Generally, gravity data interpretation is performed by assuming that the source of the anomaly has simple and ideal geometry shapes, such as a sphere, cylinder, cube, 3D prism, etc. [13]. These simple geometric shapes can be used as the building blocks of a model that represents complex geological structures. In the case of 3D sedimentary basins, the sediment layers are discretized into large numbers of 3D prisms with a fixed size laterally but adjustable vertically toward the depth according to the calculation results to represent the sediment thickness.

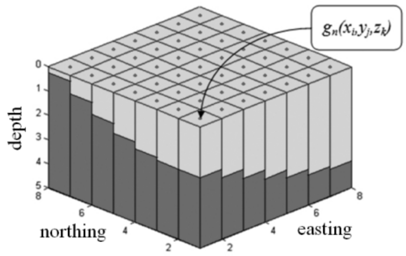

Figure 1 Discretization of sediment layers in sedimentary basins based on 3D prisms. The light-grey prisms represent the sediment layer while the dark-grey prisms correspond to the basement.

Figure 1 shows the discretization of sediment layers using 3D prisms. The light-grey prisms represent the sediment layer while the dark-grey prisms correspond to the basement. The top of each prism is fixed according to the topography, while their bottom depths are to be estimated in the inversion process. The dots on the top center of the prisms show the observation points on the surface. The gravity response of a 3D rectangular prism at a point $P(0,0,0)$ at the origin of a Cartesian coordinate system is calculated by using the equation given in Blakely [2] as follows:

$$g_z = G\Delta\rho \sum_{i=1}^{2}\sum_{j=1}^{2}\sum_{k=1}^{2} \mu_{ijk}\left[z_k \tan^{-1}\frac{x_i y_j}{z_k R_{ijk}} - x_i \log(R_{ijk}+y_j) - y_i \log(R_{ijk}+x_j) \right] \quad (1)$$

where $G = 6.67x10^{-11} m^3 kg^{-1} s^{-2}$ is the universal gravity constant, $\Delta\rho$ is the density contrast assumed to be constant for the whole sediment layer, $\mu_{ijk} = (-1)^i(-1)^j(-1)^k$, (x_i, y_j, z_k) are the east, north, and vertical (depth) directions respectively, and $R_{ijk} = \sqrt{x_i^2 + y_j^2 + z_k^2}$.

2.2 Maximum Difference Reduction (MDR)

The MDR method is essentially the same as the Bott method with an additional function called absolute maximum regularization of misfit data. The Bott method uses the Bouguer slab as a major determinant of depth perturbation, while the MDR method uses a misfit value that is normalized using absolute maximum regularization at each iteration. A flowchart of the MDR algorithm is shown in Figure 2 [10]. In the MDR method, the depth perturbation is calculated using several linked equations, i.e. Eqs. (2) to (5):

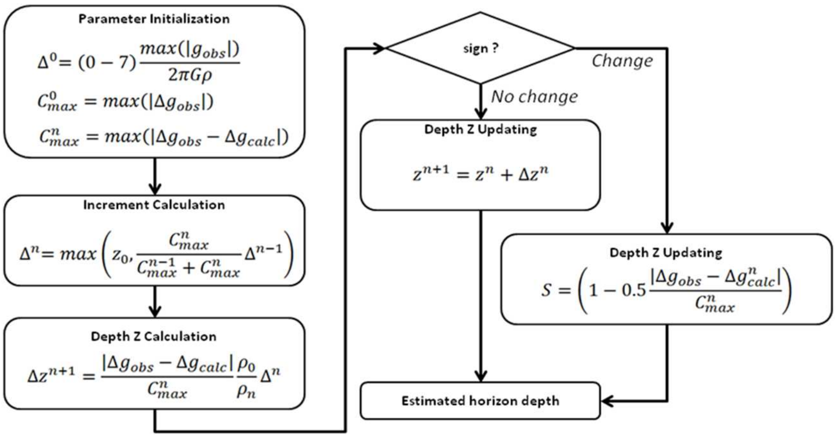

Figure 2 Flowchart of the original MDR method proposed by Zhou [10].

$$\Delta z^{n+1} = \frac{\left|\Delta g_{obs} - \Delta g^n_{calc}\right|}{C^n_{\max}}\left|\frac{\rho^0}{\rho^n}\right|\Delta^n \tag{2}$$

$$\Delta^n = \max\left(z_0, \frac{C^n_{\max}}{C^{n-1}_{\max} + C^n_{\max}}\Delta^{n-1}\right) \tag{3}$$

$$C^n_{\max} = \max\left(\left|\Delta g_{obs} - \Delta g^n_{calc}\right|\right) \tag{4}$$

$$\Delta^0 = (0-7)\frac{\max\left(\left|g_{obs}\right|\right)}{2\pi G\rho} \tag{5}$$

The MDR method starts from calculating the increment model (Eq. (3)). In the first iteration, the previous increment value is approximated using the Bouguer slab (Eq. (5)). After the increment factor is obtained, the depth perturbation calculation will follow Eq. (2). The determination of the initial value (e.g. the 0~7 value in (Eq. (5)) is based on trial and error; it does not influence the inversion results, it only affects the speed of the inversion process [10]. In our opinion, the 0~7 value is equivalent to the step size (or step length) of the gradient inversion scheme. Depth parameter updating is executed with the evaluation of the data misfit signs, whether changed or not. If the data misfit sign has not changed, the depth parameters updating will be executed using Eq. (6), but when the data misfit sign has changed, the depth parameter updating will obey the scaling down mechanism expressed in Eq. (7).

$$z_i^{n+1} = z_i^n + \Delta z_i^n \tag{6}$$

$$z^n = \left(1 - 0.5 \frac{\left|\Delta g_{obs} - \Delta g_{calc}^n\right|}{C_{\max}^n}\right) z^{n-1} \tag{7}$$

2.3 Inverse Modeling

Estimation of the basement depth or sediment thickness from gravity data is a nonlinear inverse problem. By linearizing the objective or misfit function around an initial model, iterative refinement can be performed by using model perturbations calculated from a sensitivity matrix and misfit at each iteration. Linearization of the misfit function of the nonlinear inverse problem can utilize Taylor's series expansion. The refinement of the initial model can use a local minimum approach such as the Newton method, Gauss-Newton method, Quasi-Newton method, etc. or can be done with a global minimum approach such as random search, e.g. Monte Carlo; guided random search, e.g. simulated annealing; genetic algorithm; etc. [14]. The basement depth estimation in this study is based on the local minimum approach (i.e. Gauss-Newton method). The Gauss-Newton approach considers only the first-order or linear term, such that the updated depth estimate $\mathbf{z}$ at the (n+1)-th iteration is expressed by Eq. (8):

$$\mathbf{z}_{n+1} = \mathbf{z}_n + \left[\underline{\mathbf{J}}_n^{\mathrm{T}} \underline{\mathbf{J}}_n\right]^{-1} \underline{\mathbf{J}}_n^{\mathrm{T}} \left(\mathbf{g}^{obs} - \mathbf{g}_n^{cal}\right) \tag{8}$$

where $\underline{\mathbf{J}}_n$ is the Jacobian matrix containing partial derivatives of gravity response $\mathbf{g}_i$ with respect to depth elements $\mathbf{z}_j$, i.e. $\left[\partial \mathbf{g}_i / \partial \mathbf{z}_j\right]$, i = 1, 2, 3, ... N and j = 1, 2, 3, ... M are indices for the data and model parameters respectively, while $\underline{\mathbf{J}}_n^{\mathrm{T}}$ denotes the transpose of a matrix $\underline{\mathbf{J}}_n$. In Eq. (8), both the model response $\mathbf{g}_n^{cal}$ and the Jacobian matrix $\underline{\mathbf{J}}_n$ are evaluated at the current depth model $\mathbf{z}_n$, while $\mathbf{g}^{obs}$ represent the observed gravity data.

Bott's method has been successfully transformed in the Gauss-Newton form [6]. Analogously, the incorporation of the MDR3D method in the inversion scheme can also be done by replacing the diagonal elements of the Jacobian matrix with the MDR3D formula. For this purpose, a single equation is needed to incorporate the MDR3D method in the Gauss-Newton form. The modification starts with rearranging Eqs. (6) and (2) as in Eq. (9):

$$\mathbf{z}_{n+1}^i = \mathbf{z}_n^i + \frac{C_{\max}^n}{\Delta^n}\left(\mathbf{g}^{obs} - \mathbf{g}_n^{cal}\right) \tag{9}$$

Evaluating the misfit signs is not necessary after ignoring the absolute value of the misfit $(\mathbf{g}^{obs} - \mathbf{g}_n^{cal})$ in Eq. (2). Now, Eq. (9) is sufficient to give the depth perturbation value. Eq. (9) is applicable under the assumption of constant density (for the whole sediment layer). Based on the equivalences between Eqs. (9) and (8), the MDR3D approach can be formulated in the framework of the Gauss-Newton inversion method. In this case, it can be shown that the Jacobian matrix in Eq. (8) can be represented by Eq. (10):

$$\underline{\mathbf{J}}_n = \frac{C_{\max}^n}{\Delta^n} \underline{\mathbf{I}} \tag{10}$$

where **I** is the identity matrix.

In the above inversion scheme, $\mathbf{g}^{obs}$ are supposed to be the residual anomaly, since the model's physical property is the density contrast. In fact, the observed gravity data are the Bouguer anomaly and are usually separated into regional and residual anomalies before the inversion process. Trend surface analysis (TSA) is the regional-residual anomaly separation method that is commonly used to obtain the residual anomaly with appropriate magnitude and shape for modeling [11]. We included TSA in the inversion scheme by assuming that the regional anomaly is represented by a low-order (i.e. 2^{nd} order) polynomial. The expression of $g^{reg}(x_i, y_i)$ with their coordinates (x_i, y_i) as variables is shown in Eq. (11):

$$g^{reg}(x_i, y_i) = A x_i^2 + B y_i^2 + C x_i y_i + D x_i + E y_i + F \tag{11}$$

where A, B, C, ... , F are polynomial coefficients to be determined along with the inversion for depth estimation and i = 1, 2, 3, ... N for (x_i, y_i) is the index associated with the position of the observed data. The variable with vector notation $\mathbf{g}^{reg}$ considers all elements of $g^{reg}(x_i, y_i)$.

The observed gravity data $\mathbf{g}^{obs}$ are now represented by the Bouguer anomaly $\mathbf{g}^{BA}$, while the calculated data $\mathbf{g}^{BAcalc}$ are the sum of the 3D prism gravity effect $\mathbf{g}^{3D}$ calculated by Eq. (1) and the regional anomaly $\mathbf{g}^{reg}$ calculated by Eq. (11). The Gauss-Newton approach with damping factor μ to minimize the step size of the model paramater perturbation $\Delta\mathbf{p} = (\mathbf{p}_{n+1} - \mathbf{p}_n)$ leads to the model parameter estimation at the (n+1)-th iteration expressed in Eq. (12):

$$\mathbf{p}_{n+1} = \mathbf{p}_n + [\underline{\mathbf{J}}_n^{\mathrm{T}} \underline{\mathbf{J}}_n + \mu \underline{\mathbf{I}}]^{-1} [\underline{\mathbf{J}}_n^{\mathrm{T}} (\mathbf{g}^{BA} - \mathbf{g}_n^{cal})] \tag{12}$$

where $\mathbf{p} = \begin{bmatrix} z_1 & z_2 & \cdots & z_M & A & B & \cdots & F \end{bmatrix}^T$ is the model parameter, the number of parameters being $M + 6$, and the Jacobian matrix $\mathbf{J}_n = \begin{bmatrix} \mathbf{J}_n^z & \mathbf{J}_n^{reg} \end{bmatrix}$. The expressions for $\mathbf{J}_n^z$ and $\mathbf{J}_n^{reg}$ are expressed in Eq. (13) as follows:

$$\mathbf{J}^z = \begin{bmatrix} \dfrac{\partial g_1^{3\mathrm{D}}}{\partial z_1} & \cdots & \dfrac{\partial g_1^{3\mathrm{D}}}{\partial z_M} \\ \vdots & \ddots & \vdots \\ \dfrac{\partial g_N^{3\mathrm{D}}}{\partial z_1} & \cdots & \dfrac{\partial g_N^{3\mathrm{D}}}{\partial z_M} \end{bmatrix} \text{ and } \mathbf{J}^{reg} = \begin{bmatrix} \dfrac{\partial g_1^{reg}}{\partial A} & \cdots & \dfrac{\partial g_1^{reg}}{\partial F} \\ \vdots & \ddots & \vdots \\ \dfrac{\partial g_N^{reg}}{\partial A} & \cdots & \dfrac{\partial g_N^{reg}}{\partial F} \end{bmatrix} \tag{13}$$

where, for simplicity, index n for iteration is removed and replaced by subscripts z and reg associated with depth and regional gravity respectively. The indices for components of $\mathbf{g}^{3D}$, $\mathbf{g}^{reg}$ and $\mathbf{z}$ show the number of data N and the number of model parameters involved, i.e. M for depths and 6 for polynomial coefficients.

Following Martins, *et al.* [8] and Lima, *et al.* [9], total variation regularization are also included in the inversion algorithm. In this case, the estimate of the model parameters at the $(n + 1)$-th iteration follows Eq. (14):

$$\mathbf{p}_{n+1} = \mathbf{p}_n + [\underline{\mathbf{J}}_n^{\mathrm{T}} \underline{\mathbf{J}}_n + \mu \underline{\mathbf{I}} + \mu \underline{\mathbf{H}}_n^{TV}]^{-1} [\underline{\mathbf{J}}_n^{\mathrm{T}} (\mathbf{g}^{BA} - \mathbf{g}_n^{cal}) - \mu \underline{\mathbf{J}}_n^{TV}] \tag{14}$$

where $\underline{\mathbf{J}}^{TV} = \mathbf{R}^{\mathrm{T}}\, \mathbf{q}$ and $\underline{\mathbf{H}}^{TV} = \mathbf{R}^{\mathrm{T}}\, \mathbf{Q}\, \mathbf{R}$ are the gradient vector and Hessian matrix of the approximation of the total variation function with respect to $\mathbf{p}$ evaluated at $\mathbf{p}_n$. $\mathbf{R}$ is a matrix representing the first-order discrete differential operator. The expression for the $L \times 1$ vector $\mathbf{q}$ and the $L \times L$ diagonal matrix $\mathbf{Q}$ are formulated in Eq. (15) as follows:

$$\mathbf{q} \equiv [q_l] = \frac{z_i - z_j}{[(z_i - z_j)^2 + \beta]^{1/2}} \text{ and } \mathbf{Q} \equiv [Q_{ll}] = \frac{\beta}{[(z_i - z_j)^2 + \beta]^{3/2}} \tag{15}$$

where the subscripts i and j define l-th pair of the horizontally adjacent model parameters and L is the total number of pairs (see Martins, *et al.* [8] for further details).

3 Application to Synthetics Data

The proposed method was applied to synthetic data associated with a relatively simple synthetic basin model. Gaussian noise with 0.5 mGal standard deviations was added. We used unity value for the initial parameter of the 0~7 value in Eq. 5 and the regional coefficients A~F were set to zero at the first iteration.

Figure 3 shows in general that the outline of the basin is relatively well resolved as seen from the east-west profile at x = 14 km (Figure 3(a)), except at abrupt depth transitions, shown as larger depth errors, i.e. bright colors (Figure 3(b)). The misfit of the final model was very small, leading to almost exactly superimposed contours of the synthetic data and the inverse model response (Figure 3(c) and 3(d)).

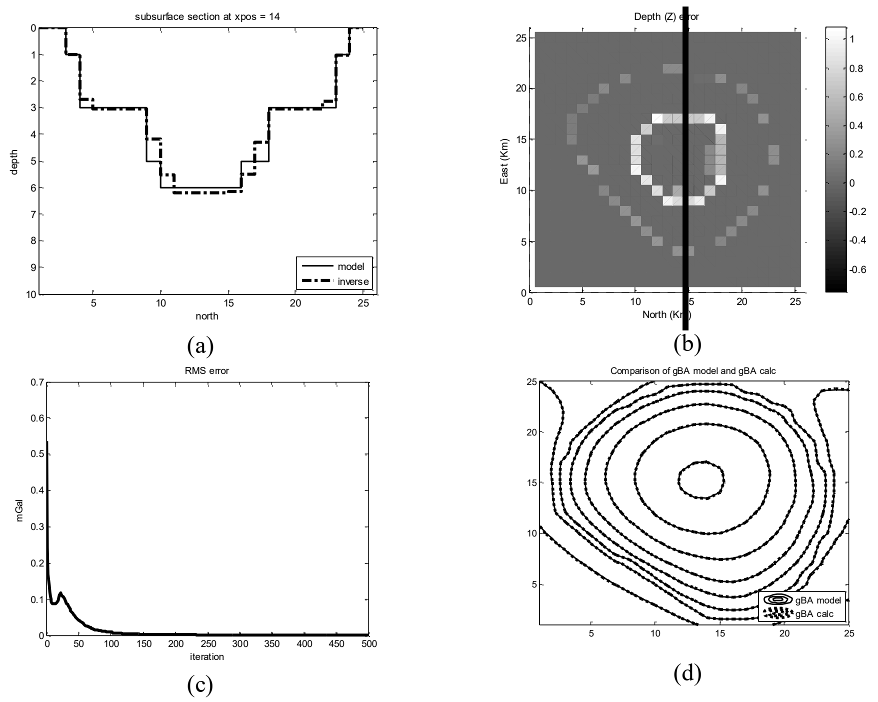

Figure 3 Inversion result using proposed method for a single interface case. (a) Comparison profile at x = 14 km of the basement model (solid line) and the inversion result (dot-dash line). (b) Depth excesses (dark) and deficiencies (light) of the inverse model relative to the synthetic model. (c) RMS error as a function of iteration. (d) Contour of synthetic data and response model at a 10-mGal interval.

Figure 4 shows the effect of the regularization parameter in suppressing the influence of noise on the final results. In this case, we have two layers in the sedimentary basin, the first layer is assumed known and fixed. It is intended to simulate the existence of other geophysical data (e.g. seismic) that can define the superficial layers in the basin. The gravity is then used to estimate the basement depth, i.e. the second interface in this case. The regularization parameters used were 1, 3, 5, and 7. It was found that the optimum regularization parameter was 7 to obtain the best basement estimation result for data with 0.5 mGal Gaussian noise. For data with more noise, greater regularization parameters should overcome the problem in the basement depth estimation. The regularization parameter can be quantitatively determined using the L-curve method [17].

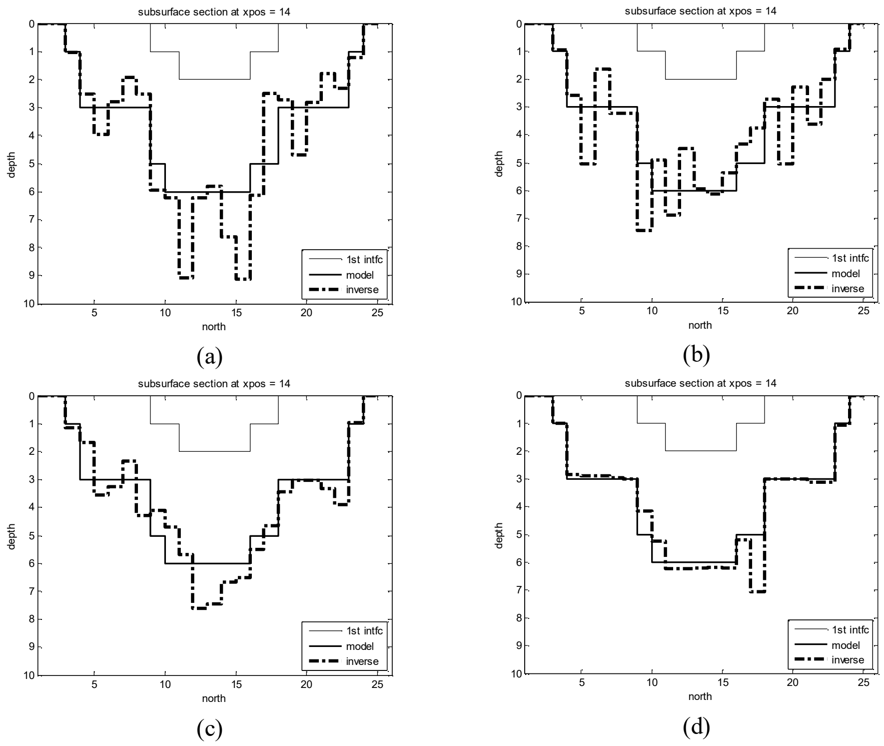

Figure 4 Basement depth estimation results for the same noise level (i.e. ±0.5 mGal) but with different regularization parameters: (a) 1, (b) 3, (c) 5, (d) 7. The sections are east-west profiles at x = 14 km.

In the previous example, using synthetic data, the estimation of the polynomial coefficients of the TSA representing the regional anomaly was also included. The results in the form of maps and profiles are not shown for the sake of conciseness of the paper. Table 1 summarizes the results with and without the inclusion of the total variation regularization. It was shown that the use of the total variation regularization allowed better recovery of the polynomial coefficients in the TSA. This indicates that the regularization improves the inversion result [9].

Table 1 Results of polynomial coefficient estimation of the regional anomaly from the synthetic data inversion in Figure 4.

Methods	A	B	C	D	E	F
Synthetics Model	-0.0210	-0.0049	-0.0100	-0.1498	-0.0724	-0.9980
MDR3D	-	-	-	-	-	-
MDR3D, TSA	0.0272	0.0433	-0.0171	-1.4682	-1.2530	9.3444
MDR3D, TSA, TVReg	-0.0179	-0.0018	-0.0106	-0.2161	-0.1350	-0.7098

4 Application to Field Data

The field gravity data used were from the Bintuni Basin, West Papua, Indonesia. The data were acquired in 2016 with a spacing interval between measurement points of ±2 km. The survey area covered the area from 132° 23' 36.4496" E to 133° 39' 3.6369" E and from 1° 48' 27.2637" S to and 2° 19' 28.1955" S at Bird's Head Peninsula, West Papua, as indicated by the white rectangle in Figure 5.

The geology of Bird's Head Peninsula is relatively complex as a result of the tectonic process in the boundary between the Australian Continental Plate and the Pacific Oceanic Plate, as shown in Figure 5. In general, the New Guinea island can be divided into several parts, namely Bird's Head and Bird's Neck (in West Papua), Bird's Body (in Papua and Papua New Guinea) and Bird's Tail (in Papua New Guinea). The Bird's Head Peninsula shows striking east-west lineaments indicated by the Sorong Fault Zone (SFZ), Yapen Fault Zone (YFZ), and Tarera-Aiduna Fault Zone. The Lengguru Fold-Thrust-Belt is dominated by northwest (NW)-southeast (SE) lineaments, especially in the Bird's Neck area [18].

The Bouguer anomaly of the survey area varies from -73 mGal up to 47.5 mGal (Figure 6). Low anomalies are concentrated in the eastern part of the survey area, while high anomalies are concentrated in the western part of the survey area. The residual gravity anomaly from the spectral analysis shows the presence of anticline structures with southeast (SE)-northwest (NW) lineament as the product of the ongoing collision between the Australian Continental Plate with the Pacific Oceanic Plate. Several sub-basins in the Bintuni Basin are also shown in Figure 7.

The basement of the Bintuni Basin in Bird's Head Peninsula consists of Mesozoic or older rock of the Australian Continental Plate in the southern part of the SFZ and Pacific Oceanic Plate at the northern part of the SFZ [19]. Its density is fairly close to the average density of the Continental Plate, i.e. 2.80 gr/cc [20]. The upper layer (or first interface) is interpreted as Klasafet and Steenkool formations consisting of soils, clays, and sands. This group is associated with the density value 2.20 gr/cc. The layer below the first interface is interpreted as the New Guinea Limestone group down to the Permian formation with a density of 2.50 gr/cc. The depth of the second interface was the target of the inversion modeling.

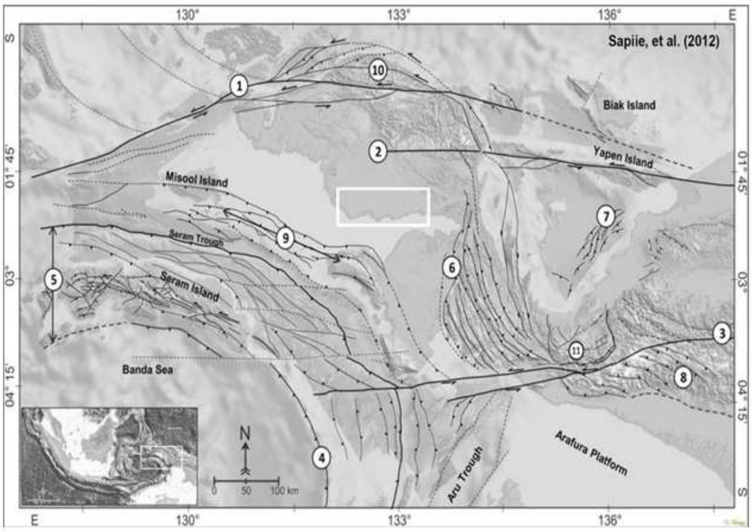

Figure 5 Geological structures in Bird's Head Peninsula, West Papua. (1) Sorong Fault Zone, (2) Yapen Fault Zone, (3) Tarera-Aiduna Fault Zone, (4) Banda Trench, (5) Seram Fold-Thrust-Belt, (6) Lengguru Fold-Thrust-Belt, (7) Cendrawasih Bay Fold-Thrust-Belt, (8) Central Range Fold-Thrust-Belt, (9) Misool-Onin-Kumawa Ridge, (10) Kemum High, (11) Weyland Overthrust [18].

Figure 9 shows the first interface depth interpreted from seismic data, while Figure 10 shows the second interface obtained from the inversion result. Both the first and the second interfaces have totally different undulations beneath the surface. The first interface is interpreted as the Top Kais Formation, while the second interface is interpreted as the Kemum Basement. Based on the inversion results, the basement depth in the survey area varies from ±2.5 km around Kamundan district up to ±7 km in the eastern part of the survey area (Manimeri district). There is a shallowing basement toward Mogoi and Kamundan from the eastern part of the survey area. The basement depth around Mogoi area is about ±4 km.

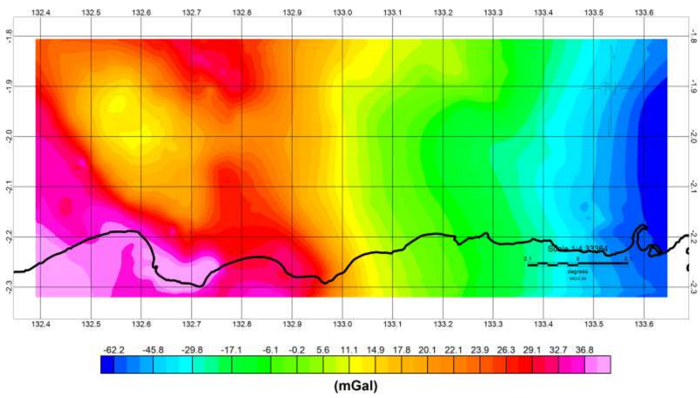

Figure 6 Bouguer anomaly map of the survey area. Low anomalies are limited only to the eastern part, while high anomalies dominate in the central and western part of the survey area.

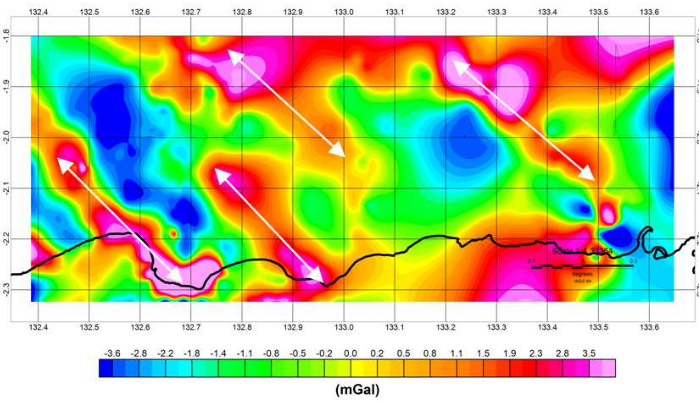

Figure 7 Residual gravity anomalies from the spectral analysis showing several sub-basins and SE-NW anticlines axis indicated by white arrows.

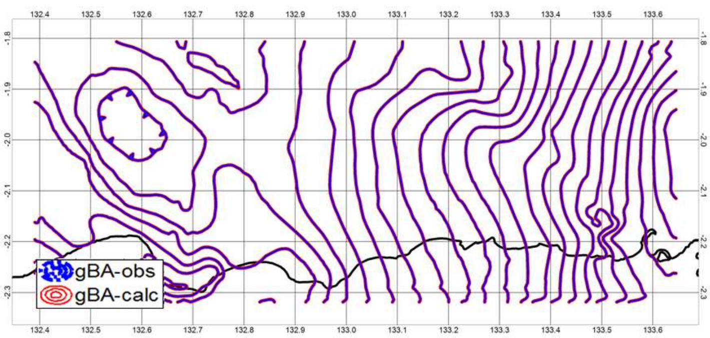

Figure 8 Contours (5 mGal interval) of the matching observed Bouguer anomalies (gBA-Obs) and the calculated Bouguer anomalies (gBA-Calc).

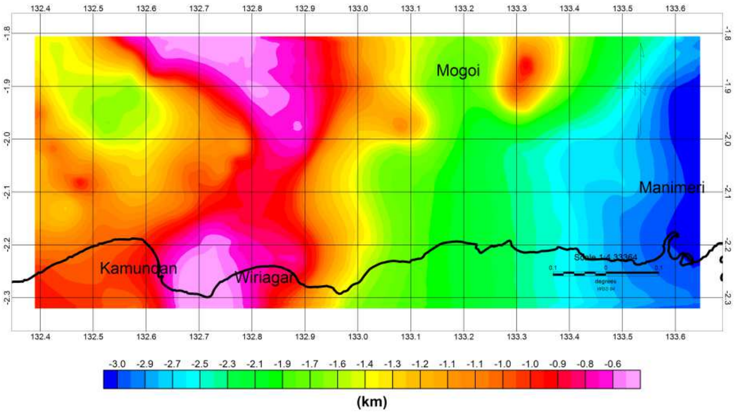

Figure 9 First interface depth associated with the Top Kais Formation, based on seismic data interpretation.

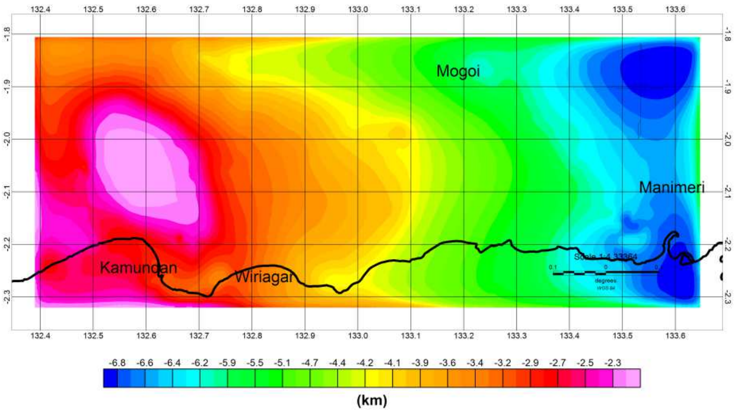

Figure 10 Second interface depth from the inversion result, showing a similar trend with the first interface depth in Figure 9, i.e. thicker sediments in the eastern part of the survey area.

The contours of both observed Bouguer anomalies and calculated Bouguer anomalies are practically identical and exactly superimposed (Figure 8), this indicates an excellent fitness between data and model response. In addition, several oil fields are found in the survey area, such as Petro Papua Mogoi Wasian (PPMW) and Petro Energi Wiriagar. The position of their production wells is consistently around the anticline structures around Mogoi and Wiriagar. These results validate the proposed inverse modeling method for the field data set.

5 Conclusions

A versatile 3D gravity inversion method for basement depth estimation was presented. The algorithm adopts a modified MDR method that was previously devised for 2D gravity inversion and recast the algorithm according to the Gauss-Newton approach. Trend surface analysis (TSA) for low-order regional anomaly estimation was also included in the inversion algorithm. A subjective process for determining regional anomalies can be avoided and the Bouguer anomaly can be directly used as input data for inversion. The use of total variation regularization in the algorithm is crucial since it increases stability in the inversion process, especially when noise is present in the data. The method was applied to synthetic and field data with satisfactory results. It was found that the basement depth in the survey area in the Bintuni basin varies from ±2.5 km around Kamundan, ±4 km around Mogoi up to ±7.0 km in the eastern part of the survey area. The results are in good agreement with the local geology. The deepening of the basement toward the east was also obtained from the modeling of airborne gravity and magnetic data partly covering the present survey area [21].

Acknowledgements

The authors are most grateful to the Centre of Geological Survey (PSG), Indonesia for their permission to use the gravity and seismic data in this study. We also sincerely thank the reviewers for their valuable suggestions for the improvement of this paper.

References

[1] Bott, M.H.P., *The Use of Rapid Digital Computing Methods for Direct Gravity Interpretation of Sedimentary Basins*, Geophysical Journal of the Royal Astronomical Society, **3**(1), pp. 63-67, 1960.

[2] Blakely, R.J., *Potential Theory Gravity and Magnetic Application*, Cambridge University Press, 1996.

[3] Parker, R.L., *The Rapid Calculation of Potential Anomalies*, Geophysical Journal of the Royal Astronomical Society, **31**, pp. 447-455, 1972.

[4] Oldenburg, D.W., *The Inversion and Interpretation of Gravity Anomalies*, Geophysics, **39**(4), pp. 526-536, 1974.

[5] Reamer, S.K. & Ferguson, J.F., *Regularized Two-Dimensional Fourier Gravity Inversion Method with Application to the Silent Canyon Caldera, Nevada*, Geophysics, **54**(4), pp. 486-496, 1988.

[6] Silva, J.B.C., Santos, D.F. & Gomes, K.P., *Fast Gravity Inversion of Basement Relief*, Geophysics, **79**(5), pp. G79-G91, 2014.

[7] Zhdanov, M.S., *Geophysical Inverse Theory and Regularization Problems*, Elsevier, 2002.

[8] Martins, C.M., Lima, W.A., Barbosa, V.C.F. & Silva, J.B.C., *Total Variation Regularization for Depth to Basement Estimate: Part1 – Mathematical Detail and Applications*, Geophysics, **76**(1), pp. I1-I12, 2011.
[9] Lima, W.A., Martins, C.M., Silva, J.B.C. & Barbosa, V.C.F., *Total Variation Regularization for Depth to Basement Estimate: Part2 – Physicogeologic Meaning and Comparisons with Previous Inversion Methods*, Geophysics, **76**(1), pp. I13-I20, 2011.
[10] Zhou, X., *Gravity Inversion of 2D Bedrock Topography for Heterogeneous Sedimentary Basins Based on Line Integral and Maximum Difference Reduction Methods*, Geophysical Prospecting, **61**(1), pp. 220-234, 2013.
[11] Chakravarthi, V. & Sundararajan, N., *3D Gravity Inversion of Basement Relief – A Depth Dependent Density Approach*, Geophysics, **72**(2), pp. I23-I 32, 2007.
[12] Hinze, W.J., Von Frese, R.R.B. & Saad, A.H., *Gravity and Magnetic Exploration: Principles, Practices and Applications*, Cambridge University Press, 2013.
[13] Telford, W.M., Geldart, L.P. & Sheriff, R.E., *Applied Geophysics 2nd edition*, Cambridge University Press, 2004.
[14] Grandis, H., *Introduction to Geophysical Inversion Modeling*, HAGI, Jakarta, 2009. (Pengantar Pemodelan Inversi Geofisika)
[15] Meju, M.A., *Geophysical Data Analysis: Understanding Inverse Problem Theory and Practice*, Society of Exploration Geophysicists, 1994.
[16] Tarantola, A., *Inverse Problem Theory and Methods for Model Parameter Estimation*, Society for Industrial and Applied Mathematics, Philadelphia, United States, 341 pp., 2005.
[17] Menke, W., *Geophysical Data Analysis: Discrete Inverse Theory*, Academic Press, Waltham, United States, 293 pp., 2012.
[18] Sapiie, B., Naryanto, W., Adyagharini, A.C. & Pamumpuni, A., Geology and Tectonic Evolution of Bird Head Region Papua, Indonesia: Implication for Hydrocarbon Exploration in Eastern Indonesia, Search & Discovery Article, No. 30260, adapted from AAPG International Convention and Exhibition, Singapore, 2012.
[19] Ikhwanudin, F. & Abdullah, C.I. *Indication Strike Slip Movement a Part of Sorong Fault Zone in Yapen Island, Papua, Indonesia*, GSTF Journal of Geological Sciences (JGS), **2** (1), pp. 25-33, 2015.
[20] Haddad, D. & Watts, A. B., *Subsidence History, Gravity Anomalies, and Flexture of The NorthEast Australian Margin in Papua New Guinea*, Tectonics, **18** (5), pp. 827-842, 1999.
[21] BP Berau Ltd., *Airborne Gravity and Magnetic Data Reprocessing, Merging and Interpretation of Bird's Head Area, Papua, Indonesia.* (Unpublished internal report).